ADVANCED MATERIALS
www.advmat.de

Porosimetry for Thin Films of Metal–Organic Frameworks: A Comparison of Positron Annihilation Lifetime Spectroscopy and Adsorption-Based Methods

*Timothée Stassin, Rhea Verbeke, Alexander John Cruz, Sabina Rodríguez-Hermida, Ivo Stassen, João Marreiros, Mikhail Krishtab, Marcel Dickmann, Werner Egger, Ivo F. J. Vankelecom, Shuhei Furukawa, Dirk De Vos, David Grosso, Matthias Thommes, and Rob Ameloot**

Thin films of crystalline and porous metal–organic frameworks (MOFs) have great potential in membranes, sensors, and microelectronic chips. While the morphology and crystallinity of MOF films can be evaluated using widely available techniques, characterizing their pore size, pore volume, and specific surface area is challenging due to the low amount of material and substrate effects. Positron annihilation lifetime spectroscopy (PALS) is introduced as a powerful method to obtain pore size information and depth profiling in MOF films. The complementarity of this approach to established physisorption-based methods such as quartz crystal microbalance (QCM) gravimetry, ellipsometric porosimetry (EP), and Kr physisorption (KrP) is illustrated. This comprehensive discussion on MOF thin film porosimetry is supported by experimental data for thin films of ZIF-8.

1. Introduction

Crystalline and porous metal–organic frameworks (MOFs) are built up from metal ion nodes interconnected by organic linkers. MOFs display record-breaking specific surface areas (up to >6000 $m^2\ g^{-1}$) and unique capacities for selective molecular uptake based on a uniform pore size combined with a high-affinity, functionalizable pore interior.[1,2] MOFs are typically synthesized as powders for bulk applications such a gas separation and storage, or catalysis.[3–5] In addition, there is tremendous potential in the use of MOF thin films as membranes, active sensor coatings, high-performance dielectrics, and other microelectronic applications that could benefit from the integration of porous functional materials.[6] Routine characterization of MOF powders typically involves N_2 physisorption to investigate their porosity and specific surface area.[7] The characterization of MOF thin films is more challenging due to the low amount of material in sub-micrometer films (**Table 1**), especially compared to the mass and volume of the substrate (e.g., a Si wafer), and often requires dedicated methods and instruments. Therefore, often only qualitative porosity characterization has been performed, e.g., through intercalation of fluorescent dyes or other labels.[8,9]

Thus far, quantitative porosimetry of MOF films has relied on physisorption, by measuring the adsorbed quantity of a probe molecule through manometric/volumetric (e.g., Kr physisorption, KrP), gravimetric (e.g., quartz crystal microbalance, QCM) or spectroscopic (e.g., ellipsometry, EP) methods.[10] When performed as a function of the adsorptive relative pressure at

Dr. T. Stassin, Dr. R. Verbeke, A. J. Cruz, Dr. S. Rodríguez-Hermida, Dr. I. Stassen, Dr. J. Marreiros, M. Krishtab, Prof. I. F. J. Vankelecom, Prof. D. De Vos, Prof. R. Ameloot
Centre for Membrane Separations, Adsorption Catalysis and Spectroscopy for Sustainable Solutions (cMACS)
KU Leuven
Celestijnenlaan 200F, Box 2454, Leuven 3001, Belgium
E-mail: rob.ameloot@kuleuven.be

Dr. M. Dickmann, Dr. W. Egger
Institut für Angewandte Physik und Messtechnik LRT2
Universität der Bundeswehr München
Werner-Heisenberg-Weg 39, Neubiberg 85577, Germany

Dr. M. Dickmann
Heinz Maier Leibnitz Zentrum (MLZ)
Technische Universität München
Lichtenbergstraße 1, Garching 85748, Germany

The ORCID identification number(s) for the author(s) of this article can be found under https://doi.org/10.1002/adma.202006993.

Prof. S. Furukawa
Institute for Integrated Cell-Material Sciences (WPI-iCeMS)
Kyoto University
iCeMS Research Building, Yoshida, Sakyo-ku, Kyoto 606-8501, Japan

Prof. D. Grosso
Aix Marseille Université
Université de Toulon
CNRS
IM2NP
Marseille 13397, France

Prof. M. Thommes
Institute of Separation Science and Technology
Department of Chemical and Bioengineering
University of Erlangen-Nuremberg
Egerlandstrasse 3, Erlangen 91058, Germany

DOI: 10.1002/adma.202006993

Table 1. Comparison of MOF powder and thin film characteristics, and suggested characterization methods.

	MOF powders[a)]	MOF films[a)]
Typical synthesis batch	100 mg	0.01 mg (100 nm × 1 cm² film)
Pore volume	0.05 cm³	5×10^{-6} cm³
Absolute surface area	100 m²	0.01 m²
State	Pure compound	Supported on a substrate
Porosity	N_2, Ar physisorption	Positron annihilation lifetime spectroscopy (PALS) Kr physisorption (KrP) Ellipsometric porosimetry (EP) with a vapor probe molecule Quartz crystal microbalance (QCM) with a vapor probe molecule

[a)]Calculated for a typical MOF density (1 g cm^{-3}), specific surface area (1000 m² g^{-1}) and pore volume (0.5 cm³ g^{-1}).

a constant temperature, an adsorption/desorption isotherm is obtained from which metrics such as the pore volume and specific surface area can be derived using appropriate models.[11] In contrast, positron lifetime annihilation spectroscopy (PALS) avoids the use of molecular probes. Instead, samples are bombarded with positrons, i.e., the electron anti-particle, whose interactions with the porous medium allow to determine pore sizes.[12,13] PALS measurements have been successfully performed on thin films of porous materials[14] as diverse as silica,[15,16] zeolites,[17] carbon,[18,19] and polymers.[20,21] While early reports have proven the suitability of PALS for crystalline and glassy MOF powders,[22,23] the potential of the method for MOF thin film porosimetry has not yet been explored and its capabilities have not yet been compared to those of adsorption-based methods. Here, we i) report the first PALS measurements on MOF thin films, ii) discuss the use and potential of PALS for MOF thin film porosimetry, iii) compare PALS to KrP, EP and QCM and iv) show the complementarity of the different methods using data measured on a 30 nm thin film of the prototypical metal–organic framework ZIF-8.[24]

2. Positron Annihilation Lifetime Spectroscopy

2.1. Positron and Positronium

Positrons (e^+) are the anti-particle of electrons (e^-); they have the same mass but opposite charge. Positrons naturally originate from positron-emitting radioactive sources (^{22}Na) or can be generated via (e^+e^-) pair production in nuclear facilities. Inside a sample, a positron is annihilated when it encounters an electron, converting their combined mass into energy that is emitted as gamma rays. The lifetime of a positron implanted in a material depends strongly on its environment. After implantation and thermalization by inelastic scattering processes, the positrons will diffuse through the material and annihilate (so-called "intrinsic" or "free e^+" annihilation). Under specific conditions that can occur inside materials containing free-volume elements or pores (e.g., polymers, silica, MOFs), the positron can form a positron-electron bound state called positronium (Ps). The latter exist as

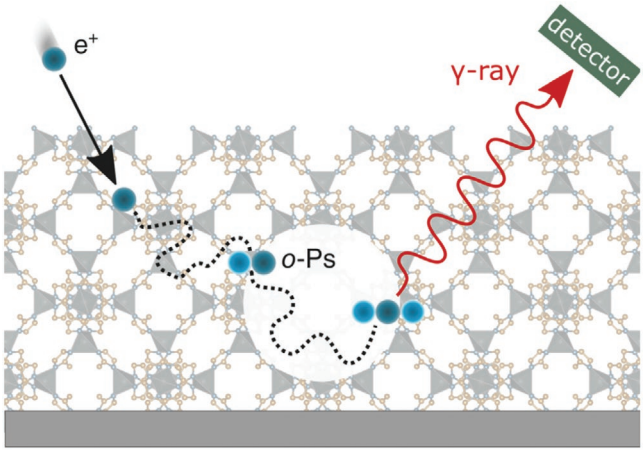

Figure 1. Positron annihilation lifetime spectroscopy (PALS) on porous materials is based on positronium "pick-off" annihilation in a pore. A positron (e^+, dark blue) is implanted and can form an *ortho*-positronium (bound state, *o*-Ps) with an electron (e^-, light blue). The lifetime of the *o*-Ps gives information about the pore size. PALS measures the time between positron implantation and the gamma-rays emitted upon pick-off annihilation.

para-Ps (*p*-Ps, singlet state) and *ortho*-Ps (*o*-Ps, triplet state), with a lifetime in vacuum of 125 ps and 142 ns, respectively.[25,26] Given the self-annihilation process and, therefore, the extremely short lifetime of the *p*-Ps, only the *o*-Ps are suitable for free-volume analyses. The *o*-Ps annihilates when it encounters an electron from the surrounding environment with an opposite spin in a process called "pick-off annihilation" (**Figure 1**).[27] The pick-off lifetime varies with the material and is characteristic for the pore size: the larger the pore, the longer the pick-off lifetime.[12]

2.2. PALS

Positron annihilation lifetime spectroscopy (PALS) measures the emitted gamma rays to determine the time between positron implantation and annihilation. A PALS spectrum is an accumulation of millions of annihilation events and consists of: i) a sum of exponential decays, convoluted ii) with the instrument resolution function, and iii) a constant background (**Figure 2**b). Every exponential decay corresponds to a different annihilation process (free e^+, *p*-Ps or *o*-Ps pick-off) with a specific lifetime and intensity. For porous materials, every pick-off lifetime corresponds to an average pore size, and the signal intensity can be related to the pore volume fraction. These properties make PALS a powerful non-destructive technique to characterize porous materials.

The depth probed by PALS is a function of the positron implantation energy and the material density. The higher the positron energy, the deeper its mean implantation depth, but the broader the probe depth distribution (Figure 2a, Equation (1), and Section S2, Supporting Information). A conventional PALS setup uses a positron-emitting radioactive source (e.g., ^{22}Na) sandwiched between two identical samples of the material under study. As the positrons from such a source have a broad energy distribution and are highly energetic (E_{max} = 545.4 keV for ^{22}Na), only samples that are at least few millimeters thick (or that reach this minimal thickness by stacking) can be measured.[28] Additionally, noise due to positron

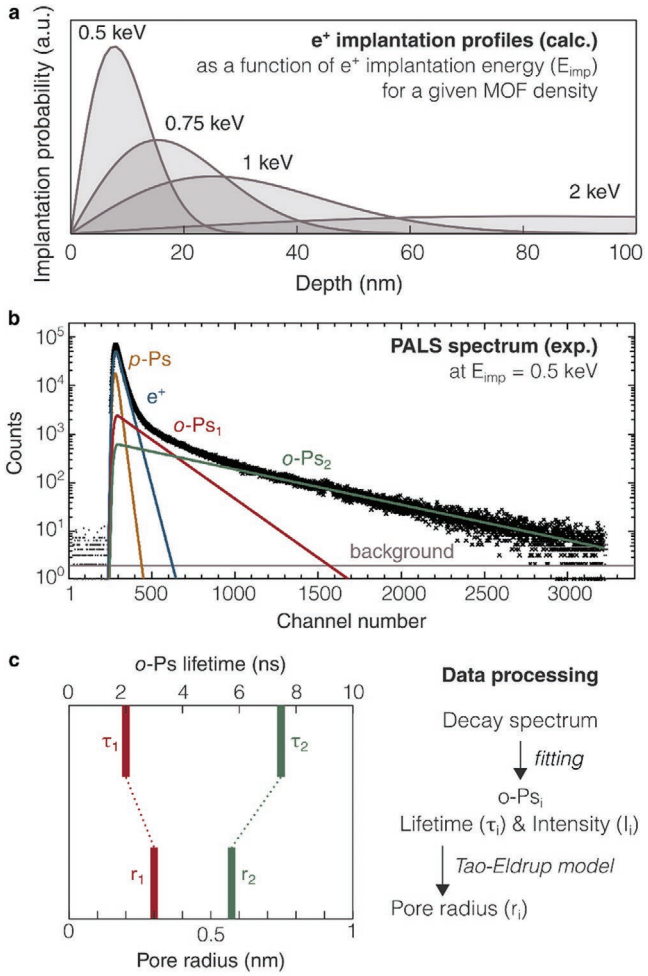

Figure 2. Implantation profile, PALS spectrum, and data processing for a ZIF-8 thin film. a) The positron implantation profile calculated for an infinitely thick ZIF-8 film (density = 0.95 g cm^{-3}) at four different positron implantation energies. b) The spectrum (gamma ray counts as a function of channel number, a measure of time) is decomposed into exponential decays corresponding to the para-positronium (*p*-Ps, brown), the free positron (e^+, blue), and at least one *o*-Ps (here two: *o*-Ps_1 and *o*-Ps_2, green and red) with distinct lifetimes and intensities, and an instrumental resolution function (sum of Gaussian curves) superimposed on a constant background (gray). c) A pore radius can be derived from an *o*-Ps lifetime using a suitable model (here: Tao–Eldrup).

annihilation within the source is unavoidable. To perform PALS on thin films, a setup that converts a continuous positron beam into a pulsed monoenergetic positron beam of low energy (<20 keV) is required.[29] Such setups allow depth profiling through a precise variation of the positron implantation energy. The beam intensity and time resolution depend on the positron source and instrument characteristics. The highest time resolution is currently obtained with the Pulsed Low Energy Positron System (PLEPS) at the NEPOMUC facility of the research nuclear reactor FRM-II in Munich (DE), where the data for this study were acquired.[30]

The positron mean implantation depth[31]

$$\tilde{z}_{1/2} = \frac{A}{\rho} \cdot E^n \quad (1)$$

with E = implantation energy (keV), sample density ρ (g cm^{-3}), A = 2.81 µg cm^{-2} keV^{-n} and n = 1.71 for polymers. So far, this value has only been determined for polymers, and is assumed to hold for MOFs.

PALS spectra are analyzed through fitting a continuous range of lifetimes (e.g., with the software packages MELT,[32] LT,[33] or CONTIN[34]), or a set of discrete lifetimes (e.g., with POSWIN,[35] PALSfit3[36]). The average pore size is obtained from discrete fitting and ideally coincides with the peak of the distribution obtained from a continuous fit. In general, the spectra of porous materials are resolved into 3 or more lifetimes (τ): the *p*-Ps (τ_1, ≈125 ps), the free e^+ (τ_2, ≈400 ps) and one or more *o*-Ps ($\tau_{3,4,...}$ < 142 ns), with respective intensities I_1, I_2, and $I_{3,4,...}$. The quality and uniqueness of the fit determine how accurately lifetimes can be resolved. Especially for fitting a continuum of lifetimes, the uniqueness is a well-known problem and the resulting pore size distributions are therefore referred to as "plausible". Discrete fitting is generally considered more robust than continuous fitting.[14] Checking fit robustness across different software packages is good practice as each one is based on a slightly different algorithm (Table S2.2, Supporting Information).

The fitted *o*-Ps lifetimes are converted into pore radii ($r_{3,4,...}$) through the Tao–Eldrup model, which assumes spherical pores,[12,13] but can be extended to different pore geometries (Figure 2c, Equation (2), and Figure S2.1: Supporting Information).[37–39] Additional porosity information can be retrieved from the *o*-Ps lifetime intensity ($I_{3,4,...}$). For example, the fractional free-volume (FFV, i.e., the fraction of unoccupied space) is calculated as $\mathrm{FFV} = \sum_{i=3}^{n} V_i \cdot I_i \cdot C$ where $V_i = \frac{4}{3}\pi \cdot r_i^3$ is the average pore volume and C is a coefficient that depends on the material chemistry, related to the probability or *o*-Ps formation inside the pores. Since the C coefficient is generally unknown, FFV's are preferably compared against a reference sample of the same composition.[40–42] The material composition (e.g., high-electron-density functional groups) can directly affect both the *o*-Ps lifetime and intensity through quenching (faster annihilation) and inhibition (reduced *o*-Ps formation probability), respectively.[43,44] It is therefore recommended to verify if the results are physically meaningful and to cross-check them with complementary methods.

The Tao–Eldrup equation

$$\tau = \frac{1}{2}\left[1 - \frac{r}{r+\Delta r} + \frac{1}{2\pi}\cdot\sin\left(\frac{2\pi \cdot r}{r+\Delta r}\right)\right]^{-1} [ns] \quad (2)$$

with Δr the empirical value for the overlap of the *o*-Ps wave function with the material around the pore. The best-fitted value equals 0.166 nm.[12,20]

2.3. PALS on MOFs

MOFs are highly suitable for PALS analysis thanks to their uniform pores. Since the first PALS measurement on MOF-5,[22] PALS has been used to characterize MOF powders with pore sizes ranging from ultramicropores (<0.7 nm) to narrow

mesopores (<2.5 nm): Al-MIL-53-Mes,[45] Al-MIL-53-Fum,[45] ZIF-8,[46] MOF-5,[47] IRMOF-3,[48] IRMOF-8,[47] MAF-6[49] (**Figure 3**). Nonetheless, understanding the behavior of positrons in MOFs and other porous materials is an active research field.[47]

The *o*-Ps lifetimes in MOFs are of two types: characteristic and non-characteristic. Characteristic lifetimes (1–28 ns for pore diameters of 0.3–2.5 nm) are related to the material structure (pore geometry, connectivity, and material composition). Non-characteristic lifetimes are usually longer and related to the material morphology (e.g., grain size). For example, in ZIF-8, two lifetimes are observed (2.0 and 7.5 ns), corresponding to two micropore sizes (0.62 and 1.15 nm) (Figure 2 and Table S2.1: Supporting Information). The large micropore size is in perfect agreement with the largest spherical void calculated for the ZIF-8 crystal structure (1.16 nm). The smaller micropore size is larger than the ZIF-8 pore window (0.34 nm), but similar to the empirical value (0.71 nm) from electron paramagnetic resonance spectroscopy (EPR) of differently sized guest molecules in contact with TEMPO-loaded ZIF-8.[24,50,51] These two lifetimes are thus characteristic for the ZIF-8 structure. Spectra of MOF-5 have also been fitted with two lifetimes. The first (13.5 ns, 1.28 nm) matches the shortest cluster-to-cluster distance (1.29 nm), and is thus characteristic for MOF-5. The second (≈80 ns, ≈6 nm) was first thought to result from defects in the material, but was later shown to result from annihilation in the intergranular space, and is thus non-characteristic.[52]

When investigating a material for the first time with PALS, some pitfalls in the data interpretation can be encountered. For example, the presence of a non-characteristic lifetime will influence the values obtained for the characteristic lifetimes (Table S2.1, Supporting Information).[53] Also, a lifetime or its intensity can be reduced by quenching (e.g., by the halogen atoms in ZIF-71 and Cl-substituted ZIF-8, Table S2.3: Supporting Information) and inhibition (e.g., Cu-CAT-1, Figure S2.3: Supporting Information), respectively. Characteristic lifetimes should thus be considered as a "MOF fingerprint". Their values should be established from PALS measurements of well-characterized reference samples, and the corresponding pore sizes compared with values obtained with other methods (e.g., Ar physisorption on powder at 87 K), or calculations based on the crystal structure (e.g., Monte Carlo, molecular dynamics, or density functional theory).[10,51,54]

Besides the pore size characterization of MOFs,[55,56] other usages of PALS have been demonstrated in literature. Pore size changes upon chemical treatment[57,58] (e.g., lithiation) or thermal treatment[59,60] (e.g., pore activation, framework amorphization) have been investigated. The degree of filling of ZIF-8 with a dye molecule and the location of metal nanoparticles in MIL-101 were indicated by the reduction in pore size observed from PALS measurements at different loadings.[61,62] In situ studies under variable temperature and atmosphere have been performed, contrasting with routine PALS measurements taking place at room conditions or in UHV. For example, the degradation of MOF-5 was followed as a function of temperature or exposure to water vapor, and adsorption isotherms were measured.[22,48]

2.4. PALS on MOF Films

Compared to manometric/volumetric or gravimetric physisorption methods, PALS offers considerable flexibility regarding the material form and the sample quantity. PALS has been performed on MOF powders,[22] glasses,[23] and fillers,[63] or toplayers[64] in membranes. As we show here, PALS can equally

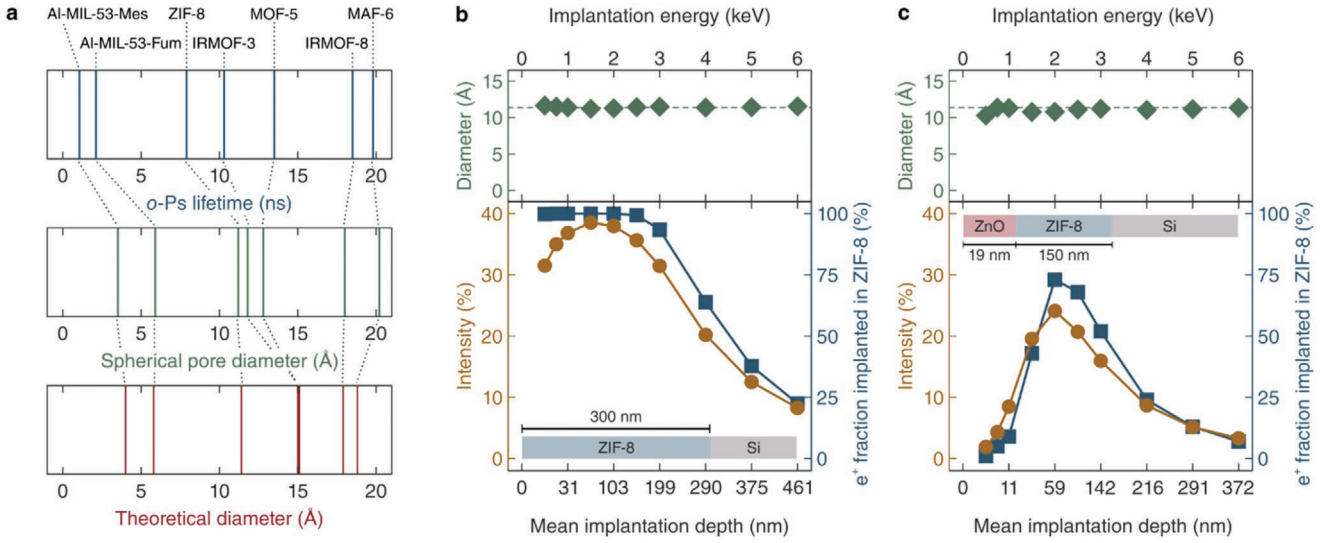

Figure 3. PALS measurements on MOF thin films. a) Characteristic *o*-Ps lifetimes, corresponding spherical pore diameters according to the Tao–Eldrup model, and crystallographic pore diameters calculated using Zeo++, for selected MOFs (see also Table S2.5 in the Supporting Information). b) Depth profiling of a 300 nm ZIF-8 thin film on Si: spherical pore diameter (green) and intensity (brown), and the simulated fraction of e^+ implanted in the ZIF-8 layer (blue), as a function of implantation energy. c) Depth profiling of a 19 nm ZnO on 150 nm ZIF-8 thin film on Si: spherical pore diameter (green) and intensity (brown), and the simulated fraction of e^+ implanted in the ZIF-8 layer (blue), as a function of positron implantation energy. For (b) and (c) the mean implantation depth is indicated for each implantation energy, and the ZIF-8 crystallographic pore diameter is plotted for comparison (green, dashed).

well be applied on ultrathin MOF films ($100 \geq d \geq 20$ nm, with the lower limit defined by the lowest implantation energy currently achievable by PLEPS, i.e., 0.5 keV). A pulsed monoenergetic positron beam of low energy is required to maximize positron implantation in the MOF film instead of in the substrate. As a demonstration, we performed PALS measurements on a 30 nm ZIF-8 film on a Si substrate with a positron implantation energy E of 0.5 keV (mean implantation depth $\tilde{z}_{1/2}$ of ≈10 nm, see Equation (1)). The obtained lifetimes are in perfect agreement with the values obtained for reference powders (Table S2.1, Supporting Information). Moreover, depth profiling of a 300 nm ZIF-8 film on Si through variation of the positron energy evidences the ZIF-8 homogeneity over the film thickness by the constant lifetime (Figure 3b). The intensity is not constant and reaches a maximum at intermediate energies. At low energies, the intensity is reduced due to surface effects (e.g., back-scattering and back-diffusion of the positrons and *o*-Ps[65–67]), while at high energies a significant fraction of the positrons passes through the MOF film and reaches the Si substrate.

Since PALS has the capability to probe the total porosity (i.e., both accessible and non-accessible), the method has been used on MOF powders to prove the formation of surface barriers that prevent porosity evaluation by physisorption.[59,68] Similarly, our results on PALS depth-profiling a 150 nm ZIF-8 film coated with a dense 19 nm ZnO layer show that non-accessible porosity in MOF films can be probed as well this way. The results show the presence of the buried porous ZIF-8 layer through its characteristic lifetime. Moreover, the intensity of the ZIF-8 lifetime matches the calculated fraction of positrons implanted in the layer (Figure 3c).

3. Physisorption-Based Porosimetry Methods

3.1. General Considerations

Physisorption of a probe molecule (the adsorptive) on a material under investigation (the adsorbent) involves van der Waals forces, i.e., weak intermolecular forces such as attractive dispersion forces, short-range repulsive forces, and specific molecular interactions (polarization, field-dipole, etc.).[11] The fluid in the adsorbed state is called the adsorbate. Physisorption-based porosimetry relies on the measurement of the equilibrium adsorbed quantity at a specific relative pressure (**Figure 4**). Typically, a controlled amount of adsorptive is dosed into a temperature-controlled measurement cell, and the uptake is quantified as the headspace pressure reduction (volumetric), sample mass increase (gravimetric) or refractive index increase (optical). If the measurement is repeated at several relative pressures at constant temperature, an adsorption isotherm is obtained. Through models that describe the adsorbed amount as a function of partial pressure, adsorbent characteristics such as the specific surface area, pore volume, and pore size distribution can be derived from the isotherm.

The choice of the adsorptive has important consequences for the measurement setup and conditions, and the data processing. Adsorptives can be gases (e.g., N_2, Ar, CO_2, Kr) or vapors (e.g., MeOH, H_2O, toluene). Full isotherm measurements are possible with organic vapors at room temperature, although measurements are generally performed in the range $0 \leq P\,P_0^{-1} \leq 0.8\text{-}0.9$ to avoid condensation. In contrast, measurements with permanent gases below their critical point require cryogenic conditions, typically at or near their boiling point. The measurement temperature and pressure range where adsorption and pore filling occurs also influences the adsorptive diffusion kinetics and thus the required equilibration times (hours to days).[10] The physicochemical properties of the adsorbate (e.g., quadrupole moment, Lewis acid/base nature) can lead to specific interactions with the adsorbent surface and complicate the analysis.[69] A further potential drawback of physisorption at cryogenic conditions is the need for high-sensitivity pressure transducers operating at low absolute pressures.

When interpreting isotherms, a distinction must be made between mesoporous and microporous materials. In mesopores (>2 nm), phenomena such as multilayer adsorption followed by capillary condensation can occur; both adsorbent–adsorbate, and adsorbate–adsorbate interactions are important. In mesopores, capillary condensation can occur and is often accompanied by hysteresis. In contrast, in micropores (<2 nm), adsorbent–adsorbate interactions dominate, leading to overlapping adsorption and desorption branches without the formation of bulk liquid.[10,11] Accurate pore size/volume analysis of both micro- and mesopores can be obtained by applying microscopic methods based on molecular simulations or density functional theory (DFT), which allow to describe the configuration of the adsorbed phase at the molecular level. These methods are based on the calculation of sets of theoretical isotherms for pairs of adsorbate/adsorbent with different pore widths and shapes called "kernels", to which the experimental isotherm can be compared.[10,11] In contrast, macroscopic thermodynamic methods such as methods based on the Kelvin equation (e.g., Barrett–Joyner–Halenda (BJH) for mesopore analysis, or the Horvath–Kawazoe (HK) and Saito–Foley methods (SF)

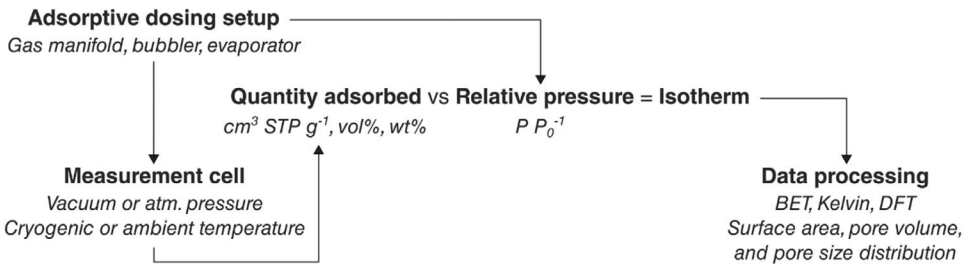

Figure 4. Flow chart for a prototypical physisorption-based porosimetry measurement.

for micropore analysis) dramatically underestimate the pore size. For instance, the BJH method breaks down for narrow mesopores (<10 nm); the pore size is underestimated by 20–30%.

A straightforward determination of the total pore volume is possible if the isotherm becomes (nearly) horizontal at high relative pressures (i.e., Type I and Type IV adsorption isotherms according to the 2015 IUPAC recommendation).[11] In this case the pore volume can be obtained from the adsorbed amount by assuming a bulk liquid state for the adsorbate (i.e., the Gurvich rule).[70] The micropore volume can be determined by the application of DFT-based methods or comparison plot approaches such as the t-plot or α_s-plot method.[10]

Surface area assessment is often performed by the Brunauer–Emmett–Teller (BET) method (Equations (3) and (4)). For nonporous, macroporous or mesoporous solids (i.e., giving a well-defined Type II or Type IV(a) isotherm), the BET area can be regarded as a true physical surface area, i.e., "probe-accessible" area. On the other hand, extreme caution is necessary if micropores are present (i.e., with pure Type I isotherms, or combinations with Types II or IV). Here, the BET theory cannot properly describe the underlying adsorption mechanism and only apparent surface areas can be obtained. Further, in case micropores are present, a linear BET range is difficult to locate. A procedure suggested by Rouquerol et al. allows to determine a linear BET range in an unambiguous way using series of consistency criteria.[71–73] This procedure improves the reproducibility of the method for microporous materials, but the obtained surface area remains an apparent one. Nevertheless, this value serves as a useful fingerprint of the adsorbent.

The Brunauer–Emmett–Teller (BET) equation

$$\frac{1}{n\cdot\left(\frac{P_0}{P}-1\right)}=\frac{C-1}{n_m\cdot C}\cdot\left(\frac{P}{P_0}\right)+\frac{1}{n_m\cdot C} \tag{3}$$

where P is the equilibrium pressure, P_0 is the saturation pressure at the temperature of adsorption, n is the adsorbed gas quantity, n_m is the monolayer adsorbed gas quantity, and C is the BET constant.

The specific surface area

$$S_{BET}=n_m\cdot N_A\cdot\sigma \tag{4}$$

where N_A is the Avogadro constant and σ the molecular cross-sectional area.

3.2. Quartz Crystal Microbalance Gravimetry

The first reported and still most widely used porosimetry method for MOF thin films is gravimetric physisorption using quartz crystal microbalance (QCM) monitoring. This technique relies on thin piezoelectric quartz crystals which, when excited with an alternating voltage, oscillate at a resonance frequency that shifts ($\Delta\nu$) when the mass of the film increases due to adsorption (Δm) (**Figure 5**).[74–76] The QCM substrates are quartz disks up to 1 in. in diameter with a cut along specific crystallographic planes and coated on both sides with a metal electrode.

The Sauerbrey equation (Equation (5)) translates the frequency shift into a mass change by treating the adsorbent film as an extension of the quartz surface.[77] This equation is applicable for oscillations in air, for thin, rigid and evenly distributed adsorbent films, and for small (few percent[78]) frequency changes. For porosimetry measurements on ultrathin MOF films, these conditions are typically satisfied.[79] For measurements in liquids or for larger relative frequency changes, and for viscoelastic films that do not fully couple mechanically to the oscillating crystal, the Z-match method[80] (using additional film properties such as the shear modulus) and dissipation monitoring[81,82] are recommended, respectively.

The Sauerbrey equation

$$\Delta m=-C\cdot\Delta\nu \tag{5}$$

with C a crystal-dependent constant.

The advantages of QCM measurements are the simplicity of the measurement and the low cost of the setup, consisting of a vapor generator, a measurement cell and an electronics box. Some of these parts can even be 3D-printed and assembled from open-source models.[83] A drawback is that the characterization of the film is performed on a QCM crystal instead of a substrate more representative of the eventual application (e.g., Si wafer). The QCM crystal stability, in particular the integrity and adhesion of the metal electrodes, can limit the processing conditions (e.g., temperature, reactants), and

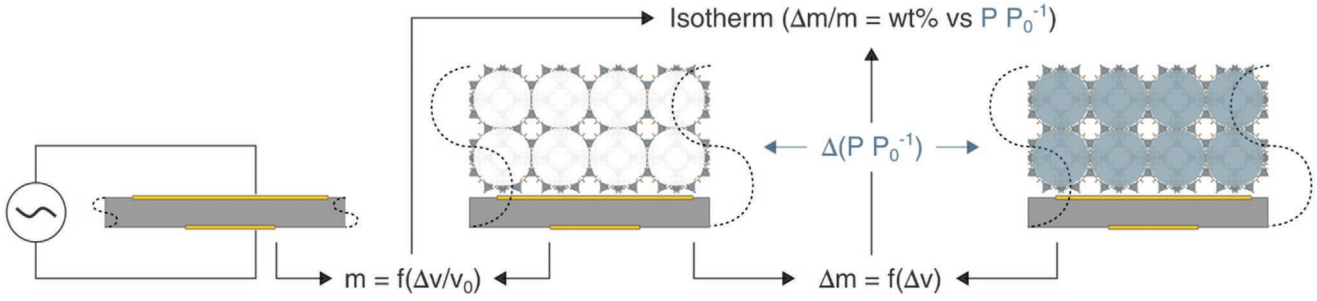

Figure 5. Quartz crystal microbalance (QCM) porosimetry. The change in resonance frequency of an oscillating quartz crystal is proportional to the mass deposited on its surface. The adsorbate mass in a porous film as a function of adsorbate relative pressure is obtained from the change in resonance frequency and can be plotted as an isotherm. The illustration is not to scale: the adsorbent film must be thin to ensure the mechanical coupling assumed in the Sauerbrey equation.

the film properties such as the crystallite orientation or the film thickness can be different. In the past, thick films were scraped off their substrate to be collected on the QCM substrate, but such a drastic intervention is not recommended because of the risks of altering the material, of including impurities, and the general issues with powders on QCM substrates (e.g., ensuring homogeneity, thickness control, and mechanical coupling).

The sensitivity of QCM measurements is determined by the quality of the electronics and the type of quartz crystal used. At room temperature, the limit of detection using standard AT-cut QCM crystals with a resonance frequency of 5–6 MHz is in the range 1–100 ng cm^{-2}, i.e., suitable for MOF ultrathin film porosimetry. Higher-frequency QCM crystals with higher sensitivity exist, but these thinner crystals become very fragile. The crystal frequency is strongly affected by the temperature, with different crystal cuts minimizing this effect at different temperatures. Careful selection of the QCM crystal and temperature control of the measurement cell are recommended.[84] Variable temperature measurements require a correction, usually based on the measurement of an uncoated QCM crystal.[85] The sensitivity of the QCM crystal is the highest in its center.[86] Frequency stabilization usually takes several minutes, and measurement of a full adsorption isotherm thus a few hours.

MOF thin films have been deposited on QCM crystals to investigate the film adsorption properties, and growth kinetics and mechanism through frequency and dissipation measurements.[87,88] Adsorption isotherms of common solvent vapors (e.g., H_2O, MeOH) have been measured and compared to isotherms measured on powder samples.[89–92] Using a high-pressure cell, measurements of CO_2, N_2, and CH_4 adsorption at temperatures between 30 and 70 °C have also been reported.[93] Moreover, diffusion coefficients of organic vapors in MOFs have been derived from time-resolved measurements of films with a precisely controlled thickness.[79,94] Orientation-dependent adsorption was investigated as well for oriented MOF films.[95]

3.3. Ellipsometric Porosimetry

In ellipsometric porosimetry (EP), ellipsometry is used to determine the quantity adsorbed by measuring the change in optical properties of a porous film (**Figure 6**).[96,97] As the pores gradually fill and empty space or gas ($n \approx 1$) is replaced by adsorbate molecules ($n > 1$), the refractive index (n) of the film increases. Ellipsometry measures the change in light polarization upon specular reflection. The two ellipsometry characteristics (Ψ and Δ) are obtained from the ratio of the reflected p- and s-polarized light (r_p, r_s), typically at various wavelengths (λ) in the visible range (Equation (6)).[98] From the raw data, the change in refractive index at each partial pressure can be extracted by building an optical model. A frequently used dispersion equation (i.e., n vs λ) is the empirical Cauchy model (Equation (7)), suitable for transparent materials, but with extensions for weakly absorbing materials,[97,99] and even metallic layers as long as their thickness is low enough to allow a portion of the incident light to pass through. For instance, investigating the porosity of thin coatings composed of complex alloys such as $Ge_{3.5}Sb_{1.0}Te_{5.5}$ is possible.[100]

The complex reflectance ratio

$$\tan(\Psi)\cdot e^{i\Delta} = \frac{r_p}{r_s} \tag{6}$$

The Cauchy model for transparent films

$$n(\lambda) = A + \frac{B}{\lambda^2} + \frac{C}{\lambda^4} \tag{7}$$

with empirical A, B, C parameters.

Several effective medium approximations (EMAs) exist to extract the adsorbate volume fraction (V) from the refractive index measured as a function of partial pressure (n_f), that of the activated adsorbent (n_s), and that of the adsorbate (n_{ads}) (Equation (8)). The Lorentz–Lorentz (Equation (9)), Maxwell–Garnett,

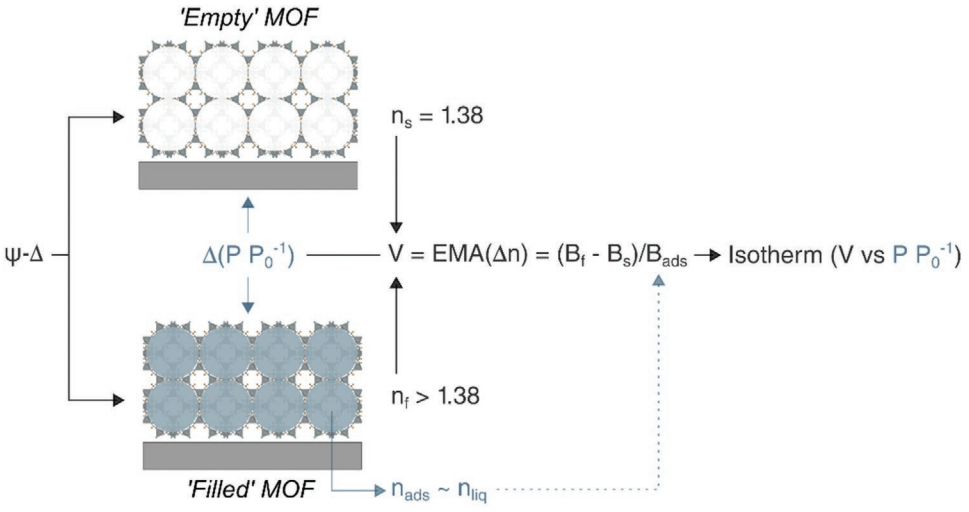

Figure 6. Ellipsometric porosimetry (EP). The refractive index as a function of adsorbate relative pressure is obtained by fitting the raw data with dispersion equations. An effective medium approximation (EMA) equation is then used to convert the refractive index into an adsorbate quantity, which can be plotted as an isotherm. Refractive index values for ZIF-8 at a wavelength of 633 nm are given as an example.

and Bruggeman EMA equations are commonly applied to process EP data.[96,101–103] These EMAs allow plotting the quantity adsorbed as a function of the relative pressure, instead of merely the refractive index or Ψ–Δ raw data. If the refractive index or Ψ–Δ raw data are plotted, it is conventional to do so at 633 nm, the operating wavelength of HeNe laser ellipsometers.

The volumetric uptake

$$V = \frac{B_f - B_s}{B_{ads}} \tag{8}$$

The Lorentz–Lorentz equation

$$B = \sum N_i \cdot \alpha_i = \frac{3\left(n^2 - 1\right)}{4\pi\left(n^2 + 2\right)} \tag{9}$$

where B is the polarizability of a unit of volume, N_i and α_i are the number of molecules and the molecular polarizability of the material components, respectively.

Describing a porous film with partially filled pores with an EMA would require three components: the volume taken up by the framework, the adsorbate and the empty space. To simplify this situation, measurements at extreme partial pressures ($P\ P_0^{-1} = 0$ and $P\ P_0^{-1} \approx 1$) are used (Figure 6). When the pores are empty ($P\ P_0^{-1} = 0$), n_f is equal to n_s. When the pores are full ($P\ P_0^{-1} \approx 1$), n_f is determined by n_s and n_{ads}. At intermediate degrees of pore filling, a simple, two-component EMA is used considering the "empty" and "filled" material as two different ones. This way, at each partial pressure, the volume of adsorbate is deduced from the volume fraction of "filled" material multiplied by the total pore volume of the adsorbent. The latter can be extracted from the ellipsometry data or other methods. Although nanoconfinement can change the refractive index of the adsorbate (n_{ads}) compared to that of the bulk liquid, this effect is usually neglected in these calculations for simplicity. Isotherms of different samples of the same material (e.g., ZIF-8) and measured with the same adsorptive can be compared as long as the values of n_s and n_{ads} are unchanged in the model.

A typical EP setup consists of a vapor generator, a measurement cell (operating in vacuum or at atmospheric pressure) with viewports at a well-defined angle, and an ellipsometer.[96,102] EP is suited for the measurement of films of thickness ranging from ≈10 nm to several µm because of the high sensitivity of the method.[97,99] As the equilibration times are short (seconds to minutes), full isotherms can be measured in 1 h. Since specular reflection is required to measure the depolarization originating from the s- and p-reflections on each interface, films can be deposited and measured on any substrate as long as they are optically flat and reflective (e.g., dielectric ceramics: glass, sapphire, SiC; semiconductors: (doped) Si, GaN, ZnO; or conductors: ITO, FTO, TiN, Au, Ag, Pt). Given the ≈0.5 × 1 cm² spot size of most spectroscopic ellipsometers (down to 25 × 60 µm² using focusing optics), small samples can be analyzed.[104] In contrast to QCM monitoring, EP is well-suited for variable temperature in situ measurements and can be used to monitor the activation process of thin porous films.[105] Another important advantage of ellipsometry is that it can differentiate the adsorbate uptake between different porous layers, which is of importance in stacked systems.[106]

EP was originally developed for mesoporous silica films.[107] For such films, the Gurvich rule is applicable, and models based on the (modified) Kelvin equation relating the pore diameter to the condensation pressure can be used to calculate pore size distributions (BJH method).[96,108] Furthermore, mechanical properties such as the Young's modulus can be derived from small and reversible film thickness changes measured during adsorption as a response to the microscopic capillary pressure and forces.[102,109] Unfortunately, this convenient method of extracting the PSD from isotherms cannot be applied to microporous systems since capillary condensation cannot take place as explained above. Therefore, PSD of microporous MOFs cannot be extracted from EP, only volume fraction of micropores. Recently, the desorption scanning mode has been adapted to EP to measure internal pore connectivity that cannot be assessed by another way.[110] This method can be used to investigate how meso- or larger pores can be connected by micropores inside the film.

EP measurements on thin films of MOFs have been carried out: i) to assess the porosity of the deposited material by comparing the measured refractive index with the (theoretical) refractive index of a dense film of similar composition,[111] ii) to prove the pore accessibility of a film and confirm the expected adsorbent properties by comparing the (shape of the) measured isotherm to isotherms measured for powders,[112–115] and iii) to evaluate the pore size based on molecular sieving of adsorptives of increasing diameter.[111,113,114]

3.4. Kr Physisorption

Static manometric/volumetric measurements rely on dosing a controlled amount of gas into a sample-containing measurement cell for which the free volume (or dead space), i.e., the space around the adsorbent, has been accurately determined for instance by using a non-adsorbing gas, typically helium (**Figure 7**). The measurement of the equilibrium pressure takes place at a fixed temperature. The amount of gas adsorbed at the equilibrium pressure is given as the difference between the amount of gas admitted and the amount of gas required to fill the free space. The quantity of adsorbed gas can thus be calculated from the corresponding pressure difference by using a proper equation of state.[10,11]

Physisorption at cryogenic conditions has been used for years for surface area determination and both micro- and mesopore size analysis.[10] N_2 adsorption at 77 K (–196 °C) has been widely used for powder measurements. However, due to the quadrupole moment of N_2 and the resulting specific interactions with surface functional groups and metal ions, the interpretation of isotherm data is not always straightforward.[11] Instead, Ar adsorption at its boiling temperature (87 K, –186 °C) is more reliable and currently recommended,[11] particularly for micropore size analysis. Ar adsorption at 87 K has the additional benefit of improved kinetics because Ar fills narrow micropores at significantly higher relative pressures in comparison with N_2 at 77 K,[69,116,117] leading to accelerated equilibration and permitting higher-resolution adsorption isotherms. Absolute surface areas as low as 0.5–1 m² can be measured using classical manometric/volumetric adsorption instrumentation with N_2 or Ar as

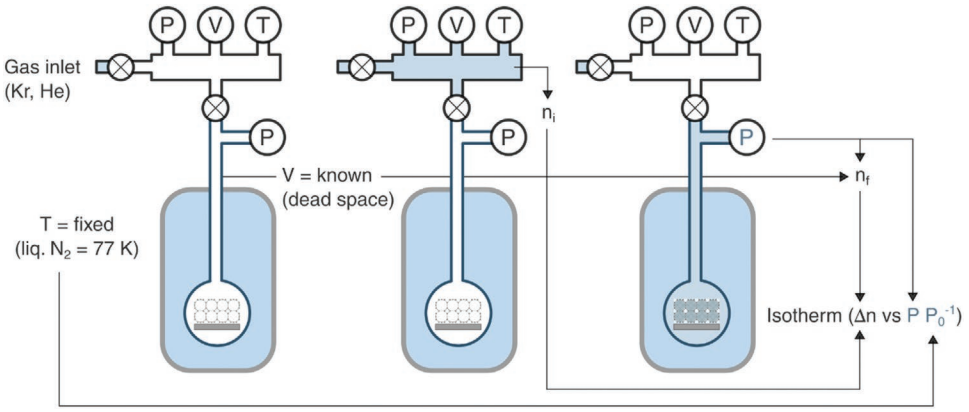

Figure 7. Volumetric physisorption measurement. A controlled amount of gas (n_i) is dosed into a measurement cell containing the sample. The cell has a known free volume and a fixed measurement temperature. The amount of gas adsorbed (Δn) is the difference between the amount of gas admitted (n_i) and the quantity of gas filling the dead space (n_f). The quantity of adsorbed gas can thus be calculated from this pressure difference and plotted as an isotherm in function of the relative pressure.

the adsorptive. The limit of detection can be further reduced to <0.05 m² when using Kr at 77 K, well below its triple point (by 38 K). At 77 K, Kr has a vapor pressure of only 0.22 kPa. Because of this extremely low saturation pressure, the number of molecules in the free volume of the measurement cell is reduced by a factor of 300 in comparison to N_2 or Ar at their respective boiling point. This change causes a significant increase in the sensitivity of Kr adsorption for analyzing samples with small absolute surface areas.[69]

To assess the surface area from a Kr isotherm measured at 77 K (Equations (3) and (4)), it is usually assumed that the adsorbate is a supercooled liquid ($P_{0,\text{liquid}} = 0.33$ kPa). Because of this convention, the maximum on the relative pressure range axis is 0.67 ($P\ P_0^{-1}/P\ P_{0,\text{liquid}}^{-1} = 0.22/0.33$). Since varying values are used for the Kr molecular footprint (0.17 nm² < σ(Kr) < 0.23 nm²), it is essential to mention the chosen values of $P_{0,\text{liquid}}$ and σ(Kr). Although Kr adsorption at 77 K is usually only used for surface area determination, some attempts to obtain pore size distributions for mesoporous oxidic films have been reported.[118] Similarly, at 87 K, pore size analysis of micro- and mesoporous thin films in the pore size range from 1–10 nm has been reported.[119–121]

3.5. Porosimetry on ZIF-8 Thin Films: Comparison of Experimental Results

Comparison of the porosimetry methods was achieved through the measurement of ultrathin (≈30 nm), smooth ($R_{RMS} < 5$ nm) and transparent ($n = 1.38$ at $\lambda = 633$ nm) ZIF-8 films deposited via MOF-CVD as reported elsewhere on a silicon substrate.[115] The method was adapted for deposition of near-identical films on a QCM crystal (Section S1, Supporting Information). The results are summarized in **Table 2**.

In order to measure a 30 nm ZIF-8 film by Kr physisorption in a standard narrow-neck measurement cell (diameter 1 cm), the minimal sample quantity must be ensured either by adding multiple pieces of a larger wafer, or by using a textured substrate (e.g., Si high-aspect-ratio (HAR) pillars) with an enhanced surface area.[120,122] In the latter case, conformal deposition methods are necessary, as for the present study. Because of improved diffusion kinetics in comparison to thicker films on a flat substrate, equilibration takes minutes instead of hours (Figure S5.1, Supporting Information). To measure large flat wafers directly, dedicated large-volume measurement tubes are necessary. Another way to reduce the required substrate size is to deposit thicker films.

QCM and EP measurements were performed with MeOH as a probe molecule. Adsorption isotherms were measured at room temperature in the range $0 \leq P\ P_0^{-1} \leq 0.8$. The normalized data are plotted in **Figure 8** ($-\Delta\nu$ and Δ at 633 nm for QCM and EP, respectively), while the non-normalized data can be found in the Supporting Information (Figures S3.1 and S4.1, Supporting Information). The sigmoidal shape of the isotherms is in perfect agreement with that of a reference MeOH isotherm measured volumetrically on ZIF-8 powder, and stems from adsorption at different sites: clustering near the window followed by cage filling.[123] Also the gravimetric uptake

Table 2. Summary of ZIF-8 porosimetry. Comparison of results obtained from various measurements on a ZIF-8 thin film with values from powder measurements and simulations.

			Method
Film	Pore diameter	1.15 nm	PALS
	BET area	1120 m² cm^{-3}	Kr physisorption
	MeOH uptake	9.4 mmol g^{-1}	QCM
Powder	Pore diameter	1.05–1.23 nm	PALS
	BET area	1241 m² cm^{-3}	N_2 physisorption
	MeOH uptake	11 mmol g^{-1}	MeOH physisorption
Simulations	Diameter of the largest sphere fitting in the cage	1.16 nm	Voronoi decomposition (Zeo++)
	Surface area (using Kr as probe)	1299 m² cm^{-3}	Voronoi decomposition + Monte-Carlo sampling (Zeo++)
	MeOH uptake	10–11 mmol g^{-1}	Grand canonical Monte-Carlo[123]

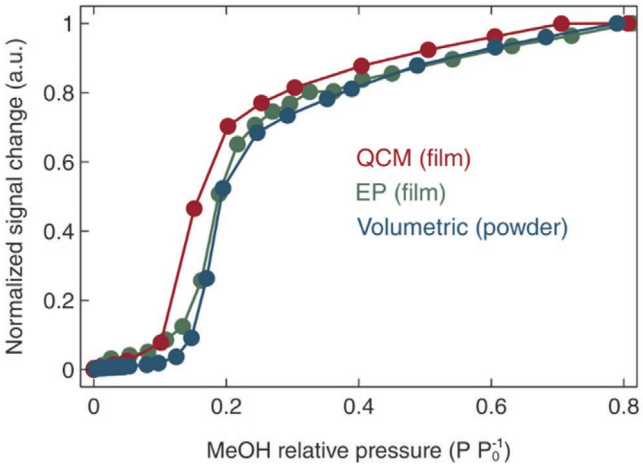

Figure 8. MeOH adsorption isotherms on ZIF-8. Volumetric measurement on ZIF-8 powder (blue), ellipsometric measurement (green) and quartz crystal microbalance gravimetric measurement (red) on a ZIF-8 thin film. Raw data (cm^3 STP, $-\Delta\nu$, Δ at 633 nm) normalized to the value at $P\,P_0^{-1} = 0.8$.

(30 wt% = 9.4 mmol g^{-1} at $P\,P_0^{-1} = 0.8$) is in line with literature values.[89] Kr adsorption was measured at 77 K and yielded a Type I isotherm, as for N_2 adsorption at 77 K on ZIF-8 powder, and as expected for a microporous material (**Figure 9**). An absolute surface area of 0.084 m² was determined by applying the BET theory and correcting for the area of a blank reference substrate and empty measurement cell. This absolute value translates to a volumetric BET surface area of 1120 m² cm^{-3} in good agreement with the theoretical value of 1299 m^2 cm^{-3} calculated via Monte Carlo sampling using Zeo++.[51]

4. Porosimetry Methods Comparison

The key aspects and possibilities of each of the four MOF thin film porosimetry methods discussed in the previous sections are summarized in **Table 3**. All methods make use

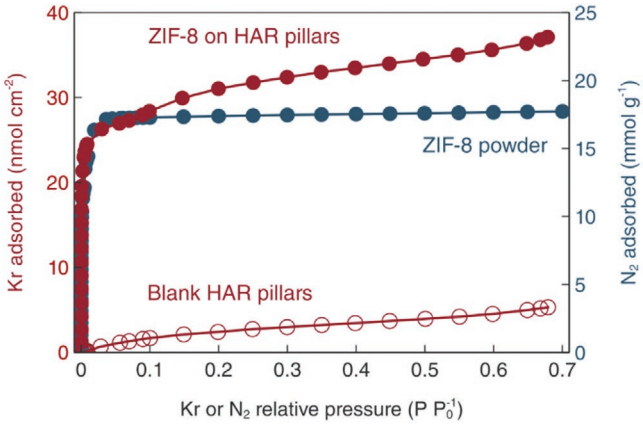

Figure 9. Kr and N_2 isotherms on ZIF-8. Volumetric measurement using Kr at 77 K on a ZIF-8 thin film conformally deposited on high-aspect-ratio (25:1) pillars (red, full dots) and on blank pillars (red, empty dots). Volumetric measurement using N_2 at 77 K on ZIF-8 powder (blue).

of probes, which are positronium for PALS (d = 1.59 Å), Kr atoms ($d_{kinetic}$ = 37 Å) for KrP and volatile organic molecules (e.g., short-chain alcohols, several Å) for both QCM and EP. Unsurprisingly, the instrumentation availability is inversely proportional to the instrumentation cost, and follows the order QCM > KrP > EP >> PALS. Each method sets different requirements with respect to the sample preparation. For all methods, the film can be measured on a substrate relevant for its implementation (e.g., a Si wafer for microelectronics applications), except for QCM which requires a dedicated substrate. EP further requires the films to be reflective and smooth. Thicker and more porous films result in higher signals, except for EP where signal generation is independent from thickness. The detection limit for the different methods cannot be compared in a straightforward way owing to the difference in measurement principle. However, all methods are sensitive enough for assessing textural properties of MOF ultrathin films (<100 nm).

Due to the use of high-energy positrons as a probe, PALS is the only method that can directly measure porosity not accessible to atomic (KrP) or molecular probes (QCM, EP). EP can give indirect information about the (non-)accessible porosity of a layer if its refractive index can be compared to the known refractive index of a dense layer of the same composition. Each method provides complementary information about the microporosity of a material: pore size and relative abundance (PALS), uptake capacity (QCM, EP), surface area and pore volume (KrP). PALS allows to probe directly as a function of depth, through selection of the positron implantation energy. EP can model stacks of layers with different porosities. PALS data processing, governing equations and models are identically applicable to micro- and mesoporous materials. In contrast, isotherm analysis methods differ for micro- and mesoporous materials, and become more complicated the smaller the pores. Nonetheless, EP and QCM measurements with probe molecules of increasing diameter can give indirect information about a micropore size based on the principle of molecular sieving. Similarly, measurements with molecules of various polarity can give information about a material's hydrophobicity. The shape of the isotherm can also hint at different pore sizes and adsorption mechanisms.

5. Conclusion

The challenging characterization of porosity in MOF thin films requires a combination of complementary methods, each with its own specificities concerning the measurement principle, instrumentation, data analysis, sample requirements and measurement conditions. Established physisorption-based methods using gases under cryogenic conditions (such as Kr) or vapors at room conditions allow to obtain information down to extremely small absolute surface areas. However, these methods exhibit limitations in evaluating the pore size in thin films of microporous materials due to the limited instrumental sensitivity and advanced methods required to analyze the data. Positronium-annihilation-based methodologies elegantly complement these physisorption-based methods by offering pore size determination and direct depth profiling.

Table 3. Comparison of different methods for MOF thin film porosimetry.

	Thin-film setup for Positron annihilation lifetime spectroscopy (PALS) Figures 1–3	Quartz crystal microbalance (QCM) Figure 5	Ellipsometric Porosimetry (EP) Figure 6	Kr physisorption (KrP) Figure 7
Method				
Principle	Annihilation	Physisorption	Physisorption	Physisorption
Class	Spectroscopic	Gravimetric	Optical	Manometric/volumetric
Raw data	Decay spectra	Resonance frequency	$\Psi(\lambda)$ and $\Delta(\lambda)$	Volume adsorbed, absolute pressures
Processed data	(*o*-)Ps lifetimes and intensities, pore diameters.	Isotherm: mass adsorbed versus relative pressure	Isotherm: refractive index, film thickness, vol% versus relative pressure;	Isotherm: volume adsorbed versus relative pressure
Governing equation or model	Tao–Eldrup and extensions	Sauerbrey	Dispersion (e.g., Cauchy), Effective Medium Approximation (e.g., Lorentz–Lorentz)	Brunauer–Emmett–Teller (BET)
Output (**Best available**)	**Pore sizes** and relative intensities, **Non-accessible porosity**, **Depth profiling**, Fractional free volume	**Uptake capacity (wt%)**, **Pore hydrophobicity**, Adsorption mechanism, Pore window cut-off size (molecular sieving),	**Uptake capacity (vol%)**, Pore window cut-off size (molecular sieving), Pore hydrophobicity, Adsorption mechanism, Swelling	**Surface area**, **Pore volume**, Adsorption mechanism (Pore size distributions not yet reported for MOFs)
Instrumentation				
Components	Pulsed low- and monoenergetic positron beam + PALS setup	Dosing setup + measurement cell + electronics box	Dosing setup + measurement cell + ellipsometer	Static manometric physisorption instrument with low pressure transducers (1 mbar)
Cost	Very high	Low	High	Moderate
Availability	Very low	High	Low	Moderate
Probe				
Class	Particle	Molecule	Molecule	Atom
Nature	Positronium	Organic vapors	Organic vapors	Kr
Size	1.59 Å	Variable	Variable	37 Å (kinetic diameter)
Sample requirements				
Substrate	Any, flat	QCM crystal	Flat, reflective	Any
Substrate area	0.5–1 cm^2	1–2 cm^2	1 cm^2	Depends on film thickness and instrument LOD
Film thickness	>20 nm	Any	>10 nm	Depends on substrate size and instrument LOD
Film roughness	Low for thin films High for thick films	Any	Low	Any
Film reflectivity	Any	Any	Yes	Any
Measurement				
Time	Several minutes per energy	1–2 h for full isotherm	1–2 h for full isotherm	Several hours for full isotherm, but only points in BET range needed for surface area determination.
Pressure	UHV	(sub-)atmospheric	(sub-)atmospheric	<2 mbar
Temperature	–190 to 300 °C	≥25 °C depending on adsorbate and QCM crystal cut	≥25 °C depending on adsorbate	–196 °C (77 K)
Spot size	1 mm^2	Not applicable (no beam).	0.5 × 1 cm^2	Not applicable (no beam)
Depth profiling	Yes, with tuneable beam energy	No	Yes, with multi-layer (graded) models	No
Spatial resolution	1 mm, or 1 µm with a scanning positron microscope	No	Yes, with focusing optics (spot size 25 × 60 μm^2) or laser, and moving stage	No
Variable temperature	Yes	Limited	Yes	No
Variable atmosphere	No	Yes	Yes	No

Supporting Information

Supporting Information is available from the Wiley Online Library or from the author.

Acknowledgements

T.S., R.V., and I.S. thank the Research Foundation Flanders (FWO) for SB-Ph.D. and postdoctoral fellowships (1S53316N, 1S00917N, and 12L5417N). R.A. thanks the European Union for the Horizon 2020 FETOPEN-1-2016-2017 research and innovation program (grant agreement No 801464, acronym: SPRINT), the European Research Council (ERC) under the European Union's Horizon 2020 research and innovation program (grant agreement No 716472, acronym: VAPORE), the Research Foundation Flanders (FWO) for research projects and grants G85720N, G0E6319N, G0H0716N, G083016N, and 1501618N, and KU Leuven for research project C32/18/056. Nathalie Wauteraerts is thanked for her kind help with KrP measurements. Max Tietze and Dmitry Kravchenko extensively assisted with the assembly and operation of the adsorptive dosing setup. Fruitful scientific discussions about QCM gravimetry were held with Min Tu. Philippe Vereecken and imec kindly provided the Si micropillars. Silvia Armini and imec generously granted access to the EP instrumentation. PALS measurements are based upon experiments performed at the PLEPS instrument operated by FRM-II at the Heinz Maier-Leibnitz Zentrum (MLZ), Garching, Germany. Funding from the German BMBF project 05K16WN1-Positec is gratefully acknowledged.

Conflict of Interest

The authors declare no conflict of interest.

Keywords

adsorption, metal–organic frameworks, porosimetry, porous materials, positron annihilation lifetime spectroscopy, thin films

Received: October 14, 2020
Revised: December 7, 2020
Published online: March 17, 2021

[1] H. Furukawa, K. E. Cordova, M. O'Keeffe, O. M. Yaghi, *Science* **2013**, *341*, 1230444.
[2] I. M. Hönicke, I. Senkovska, V. Bon, I. A. Baburin, N. Bönisch, S. Raschke, J. D. Evans, S. Kaskel, *Angew. Chem., Int. Ed.* **2018**, *57*, 13780.
[3] M. Rubio-Martinez, C. Avci-Camur, A. W. Thornton, I. Imaz, D. Maspoch, M. R. Hill, *Chem. Soc. Rev.* **2017**, *46*, 3453.
[4] A. U. Czaja, N. Trukhan, U. Müller, *Chem. Soc. Rev.* **2009**, *38*, 1284.
[5] A. Corma, H. García, F. X. Llabrés i Xamena, *Chem. Rev.* **2010**, *110*, 4606.
[6] I. Stassen, N. Burtch, A. Talin, P. Falcaro, M. Allendorf, R. Ameloot, *Chem. Soc. Rev.* **2017**, *46*, 3185.
[7] A. J. Howarth, A. W. Peters, N. A. Vermeulen, T. C. Wang, J. T. Hupp, O. K. Farha, *Chem. Mater.* **2017**, *29*, 26.
[8] P. Falcaro, K. Okada, T. Hara, K. Ikigaki, Y. Tokudome, A. W. Thornton, A. J. Hill, T. Williams, C. Doonan, M. Takahashi, *Nat. Mater.* **2017**, *16*, 342.
[9] Z. Wang, J. Liu, B. Lukose, Z. Gu, P. G. Weidler, H. Gliemann, T. Heine, C. Wöll, *Nano Lett.* **2014**, *14*, 1526.
[10] F. Rouquerol, J. Rouquerol, K. S. W. Sing, P. L. Llewellyn, G. Maurin, *Adsorption by Powders and Porous Solids: Principles, Methodology and Applications*, Elsevier/AP, Amsterdam, The Netherlands **2014**.
[11] M. Thommes, K. Kaneko, A. V. Neimark, J. P. Olivier, F. Rodriguez-Reinoso, J. Rouquerol, K. S. W. Sing, *Pure Appl. Chem.* **2015**, *87*, 1051.
[12] M. Eldrup, D. Lightbody, J. N. Sherwood, *Chem. Phys.* **1981**, *63*, 51.
[13] S. J. Tao, *J. Chem. Phys.* **1972**, *56*, 5499.
[14] D. W. Gidley, H.-G. Peng, R. S. Vallery, *Annu. Rev. Mater. Res.* **2006**, *36*, 49.
[15] D. W. Gidley, W. E. Frieze, T. L. Dull, A. F. Yee, E. T. Ryan, H.-M. Ho, *Phys. Rev. B* **1999**, *60*, R5157.
[16] D. W. Gidley, W. E. Frieze, T. L. Dull, J. Sun, A. F. Yee, C. V. Nguyen, D. Y. Yoon, *Appl. Phys. Lett.* **2000**, *76*, 1282.
[17] A. Cabral-Prieto, I. García-Sosa, R. López-Castañares, O. Olea-Cardoso, *Microporous Mesoporous Mater.* **2013**, *175*, 134.
[18] G. Kögel, D. Schödlbauer, W. Triftshäuser, J. Winter, *Phys. Rev. Lett.* **1988**, *60*, 1550.
[19] M. J. Puska, R. M. Nieminen, *J. Phys.: Condens. Matter* **1992**, *4*, L149.
[20] Y. C. Jean, *Microchem. J.* **1990**, *42*, 72.
[21] Y. C. Jean, J. D. Van Horn, W.-S. Hung, K.-R. Lee, *Macromolecules* **2013**, *46*, 7133.
[22] M. Liu, A. G. Wong-Foy, R. S. Vallery, W. E. Frieze, J. K. Schnobrich, D. W. Gidley, A. J. Matzger, *Adv. Mater.* **2010**, *22*, 1598.
[23] A. W. Thornton, K. E. Jelfs, K. Konstas, C. M. Doherty, A. J. Hill, A. K. Cheetham, T. D. Bennett, *Chem. Commun.* **2016**, *52*, 3750.
[24] K. S. Park, Z. Ni, A. P. Cote, J. Y. Choi, R. Huang, F. J. Uribe-Romo, H. K. Chae, M. O'Keeffe, O. M. Yaghi, *Proc. Natl. Acad. Sci. USA* **2006**, *103*, 10186.
[25] P. Hasbach, G. Hilkert, E. Klempt, G. Werth, *Nuovo Cimento A* **1987**, *97*, 419.
[26] T. Goworek, K. Ciesielski, B. Jasińska, J. Wawryszczuk, *Chem. Phys.* **1998**, *230*, 305.
[27] O. E. Mogensen, *Positron Annihilation in Chemistry*, Springer, Berlin/Heidelberg, Germany **1995**.
[28] C. Hugenschmidt, in *Physics with Many Positrons: Proc. of the Int. School of Physics "Enrico Fermi" Course CLXXIV*, IOS Press, Amsterdam, The Netherlands **2010**, p. 399.
[29] W. Egger, *ENFI* **2010**, *174*, 419.
[30] W. Egger, P. Sperr, G. Kögel, G. Dollinger, *Phys. Status Solidi C* **2007**, *4*, 3969.
[31] J. Algers, P. Sperr, W. Egger, G. Kögel, F. Maurer, *Phys. Rev. B* **2003**, *67*, 12.
[32] A. Shukla, M. Peter, L. Hoffmann, *Nucl. Instrum. Methods Phys. Res., Sect. A* **1993**, *335*, 310.
[33] J. Kansy, *Nucl. Instrum. Methods Phys. Res., Sect. A* **1996**, *374*, 235.
[34] R. B. Gregory, *Nucl. Instrum. Methods Phys. Res., Sect. A* **1991**, 496.
[35] D. Bochert, Master's thesis, Institut für Angewandte Physik und Messtechnik, Universität der Bundeswehr München, Munich, Germany **2014**.
[36] P. Kirkegaard, J. V. Olsen, M. M. Eldrup, PALSfit3: A Software Package for Analysing Positron Lifetime Spectra A Software Package for Analysing Positron Lifetime Spectra, **2017**.
[37] T. L. Dull, W. E. Frieze, D. W. Gidley, J. N. Sun, A. F. Yee, *J. Phys. Chem. B* **2001**, *105*, 4657.
[38] T. Goworek, *J. Nucl. Radiochem. Sci.* **2000**, *1*, 11.
[39] R. Zaleski, J. Wawryszczuk, T. Goworek, *Radiat. Phys. Chem.* **2007**, *76*, 243.
[40] H. Nakanishi, Y. C. Jean, E. G. Smith, T. C. Sandreczki, *J. Polym. Sci., Part B: Polym. Phys.* **1989**, *27*, 1419.
[41] M. Dickmann, S. Tarter, W. Egger, A. Pegoretti, D. Rigotti, R. S. Brusa, R. Checchetto, *Polymer* **2020**, *202*, 122729.
[42] S. J. Tao, *Appl. Phys.* **1976**, *10*, 67.
[43] Y. C. Jean, P. E. Mallon, D. M. Schrader, *Principles and Applications of Positron and Positronium Chemistry*, World Scientific, Singapore **2002**.
[44] S. Y. Chuang, S. J. Tao, *J. Chem. Phys.* **1970**, *52*, 749.
[45] T. Stassin, S. Waitschat, N. Heidenreich, H. Reinsch, F. Pluschkell, D. Kravchenko, J. Marreiros, I. Stassen, J. van Dinter, R. Verbeke,

M. Dickmann, W. Egger, I. Vankelecom, D. D. Vos, R. Ameloot, N. Stock, *Chem. - Eur. J.* **2020**, *26*, 10841.
[46] A. F. Bushell, M. P. Attfield, C. R. Mason, P. M. Budd, Y. Yampolskii, L. Starannikova, A. Rebrov, F. Bazzarelli, P. Bernardo, J. Carolus Jansen, M. Lanč, K. Friess, V. Shantarovich, V. Gustov, V. Isaeva, *J. Membr. Sci.* **2013**, *427*, 48.
[47] P. Crivelli, D. Cooke, B. Barbiellini, B. L. Brown, J. I. Feldblyum, P. Guo, D. W. Gidley, L. Gerchow, A. J. Matzger, *Phys. Rev. B* **2014**, *89*, 241103.
[48] P. Guo, D. Dutta, A. G. Wong-Foy, D. W. Gidley, A. J. Matzger, *J. Am. Chem. Soc.* **2015**, *137*, 2651.
[49] T. Stassin, I. Stassen, J. Marreiros, A. J. Cruz, R. Verbeke, M. Tu, H. Reinsch, M. Dickmann, W. Egger, I. F. J. Vankelecom, D. E. De Vos, R. Ameloot, *Chem. Mater.* **2020**, *32*, 1784.
[50] D. M. Polyukhov, A. S. Poryvaev, S. A. Gromilov, M. V. Fedin, *Nano Lett.* **2019**, *19*, 6506.
[51] T. F. Willems, C. H. Rycroft, M. Kazi, J. C. Meza, M. Haranczyk, *Microporous Mesoporous Mater.* **2012**, *149*, 134.
[52] D. Dutta, J. I. Feldblyum, D. W. Gidley, J. Imirzian, M. Liu, A. J. Matzger, R. S. Vallery, A. G. Wong-Foy, *Phys. Rev. Lett.* **2013**, *110*, 197403.
[53] H. B. T. Jeazet, T. Koschine, C. Staudt, K. Raetzke, C. Janiak, *Membranes* **2013**, *3*, 331.
[54] D. Dubbeldam, S. Calero, D. E. Ellis, R. Q. Snurr, *Mol. Simul.* **2016**, *42*, 81.
[55] T. Stassin, S. Waitschat, N. Heidenreich, H. Reinsch, F. Puschkell, D. Kravchenko, J. Marreiros, I. Stassen, J. van Dinter, R. Verbeke, M. Dickmann, W. Egger, I. Vankelecom, D. De Vos, R. Ameloot, N. Stock, *Chem. - Eur. J.* **2020**, *26*, 10841.
[56] S. Nandi, P. D. Luna, T. D. Daff, J. Rother, M. Liu, W. Buchanan, A. I. Hawari, T. K. Woo, R. Vaidhyanathan, *Sci. Adv.* **2015**, *1*, 1500421.
[57] M. C. Duke, B. Zhu, C. M. Doherty, M. R. Hill, A. J. Hill, M. A. Carreon, *Desalination* **2016**, *377*, 128.
[58] K. Konstas, J. W. Taylor, A. W. Thornton, C. M. Doherty, W. X. Lim, T. J. Bastow, D. F. Kennedy, C. D. Wood, B. J. Cox, J. M. Hill, A. J. Hill, M. R. Hill, *Angew. Chem., Int. Ed.* **2012**, *51*, 6639.
[59] S. S. Mondal, A. Bhunia, A. G. Attallah, P. R. Matthes, A. Kelling, U. Schilde, K. Müller-Buschbaum, R. Krause-Rehberg, C. Janiak, H.-J. Holdt, *Chem. - Eur. J.* **2016**, *22*, 6905.
[60] C. Zhou, L. Longley, A. Krajnc, G. J. Smales, A. Qiao, I. Erucar, C. M. Doherty, A. W. Thornton, A. J. Hill, C. W. Ashling, O. T. Qazvini, S. J. Lee, P. A. Chater, N. J. Terrill, A. J. Smith, Y. Yue, G. Mali, D. A. Keen, S. G. Telfer, T. D. Bennett, *Nat. Commun.* **2018**, *9*, 5042.
[61] M. Tu, H. Reinsch, S. Rodríguez-Hermida, R. Verbeke, T. Stassin, W. Egger, M. Dickmann, B. Dieu, J. Hofkens, I. F. J. Vankelecom, N. Stock, R. Ameloot, *Angew. Chem., Int. Ed.* **2019**, *58*, 2423.
[62] Y.-Z. Chen, B. Gu, T. Uchida, J. Liu, X. Liu, B.-J. Ye, Q. Xu, H.-L. Jiang, *Nat. Commun.* **2019**, *10*, 1.
[63] Q. Song, S. K. Nataraj, M. V. Roussenova, J. C. Tan, D. J. Hughes, W. Li, P. Bourgoin, M. A. Alam, A. K. Cheetham, S. A. Al-Muhtaseb, E. Sivaniah, *Energy Environ. Sci.* **2012**, *5*, 8359.
[64] J. Yuan, W.-S. Hung, H. Zhu, K. Guan, Y. Ji, Y. Mao, G. Liu, K.-R. Lee, W. Jin, *J. Membr. Sci.* **2019**, *572*, 20.
[65] H. H. Seliger, *Phys. Rev.* **1952**, *88*, 408.
[66] J. Makinen, S. Palko, J. Martikainen, P. Hautojarvi, *J. Phys.: Condens. Matter* **1992**, *4*, L503.
[67] J. Xu, J. Moxom, S. Yang, R. Suzuki, T. Ohdaira, *Chem. Phys. Lett.* **2002**, *364*, 309.
[68] J. I. Feldblyum, M. Liu, D. W. Gidley, A. J. Matzger, *J. Am. Chem. Soc.* **2011**, *133*, 18257.
[69] M. Thommes, K. A. Cychosz, *Adsorption* **2014**, *20*, 233.
[70] L. Gurvich, *J. Phys. Chem. Soc. Russ.* **1915**, *47*, 805.
[71] Y.-S. Bae, A. Ö. Yazaydın, R. Q. Snurr, *Langmuir* **2010**, *26*, 5475.
[72] K. S. Walton, R. Q. Snurr, *J. Am. Chem. Soc.* **2007**, *129*, 8552.
[73] J. Rouquerol, P. Llewellyn, F. Rouquerol, *Stud. Surf. Sci. Catal.* **2007**, *160*, 49.
[74] M. D. Ward, D. A. Buttry, *Science* **1990**, *249*, 1000.
[75] D. Johannsmann, in *The Quartz Crystal Microbalance in Soft Matter Research*, Springer International Publishing, Cham **2015**, pp. 1–22.
[76] D. Johannsmann, in *The Quartz Crystal Microbalance in Soft Matter Research*, Springer International Publishing, Cham, Switzerland **2015**, pp. 191–204.
[77] G. Sauerbrey, *Z. Phys.* **1959**, *155*, 206.
[78] D. R. Denison, *J. Vac. Sci. Technol.* **1973**, *10*, 126.
[79] O. Zybaylo, O. Shekhah, H. Wang, M. Tafipolsky, R. Schmid, D. Johannsmann, C. Wöll, *Phys. Chem. Chem. Phys.* **2010**, *12*, 8092.
[80] C.-S. Lu, O. Lewis, *J. Appl. Phys.* **1972**, *43*, 4385.
[81] G. N. M. Ferreira, A.-C. da-Silva, B. Tomé, *Trends Biotechnol.* **2009**, *27*, 689.
[82] F. Höök, M. Rodahl, P. Brzezinski, B. Kasemo, *Langmuir* **1998**, *14*, 729.
[83] "Quartz Crystal Microbalance with Dissipation Monitoring: the first scientific QCM entirely Open Source," https://openqcm.com/ (accessed: August 2020).
[84] D. Johannsmann, in *The Quartz Crystal Microbalance in Soft Matter Research*, Springer International Publishing, Cham, Switzerland **2015**, pp. 377–385.
[85] A. Rahtu, M. Ritala, *Appl. Phys. Lett.* **2002**, *80*, 521.
[86] M. Varga, A. Laposa, P. Kulha, J. Kroutil, M. Husak, A. Kromka, *Phys. Status Solidi B* **2015**, *252*, 2591.
[87] V. Stavila, J. Volponi, A. M. Katzenmeyer, M. C. Dixon, M. D. Allendorf, *Chem. Sci.* **2012**, *3*, 1531.
[88] O. Shekhah, *Materials* **2010**, *3*, 1302.
[89] K. Khaletskaya, S. Turner, M. Tu, S. Wannapaiboon, A. Schneemann, R. Meyer, A. Ludwig, G. Van Tendeloo, R. A. Fischer, *Adv. Funct. Mater.* **2014**, *24*, 4804.
[90] T. Stassin, S. Rodríguez-Hemida, B. Schrode, A. J. Cruz, F. Carraro, D. Kravchenko, V. Creemers, I. Stassen, T. Hauffman, D. E. D. Vos, P. Falcaro, R. Resel, R. Ameloot, *Chem. Commun.* **2019**, *55*, 10056.
[91] E. Biemmi, C. Scherb, T. Bein, *J. Am. Chem. Soc.* **2007**, *129*, 8054.
[92] E. Virmani, J. M. Rotter, A. Mähringer, T. von Zons, A. Godt, T. Bein, S. Wuttke, D. D. Medina, *J. Am. Chem. Soc.* **2018**, *140*, 4812.
[93] A. Venkatasubramanian, M. Navaei, K. R. Bagnall, K. C. McCarley, S. Nair, P. J. Hesketh, *J. Phys. Chem. C* **2012**, *116*, 15313.
[94] W. Zhou, C. Wöll, L. Heinke, *Materials* **2015**, *8*, 3767.
[95] B. Liu, M. Tu, R. A. Fischer, *Angew. Chem., Int. Ed.* **2013**, *52*, 3402.
[96] M. R. Baklanov, K. P. Mogilnikov, V. G. Polovinkin, F. N. Dultsev, *J. Vac. Sci. Technol., B: Microelectron. Nanometer Struct.–Process., Meas., Phenom.* **2000**, *18*, 1385.
[97] H. Fujiwara, *Spectroscopic Ellipsometry: Principles and Applications*, John Wiley & Sons, New York **2007**.
[98] H. G. Tompkins, *A User's Guide to Ellipsometry*, Academic Press, Boston, MA, USA **1993**.
[99] H. Tompkins, E. A. Irene, *Handbook of Ellipsometry*, William Andrew, Norwich, NY, USA **2005**.
[100] C. Rebora, R. Huang, G. P. Kissling, M. Bocquet, K. D. Groot, L. Favre, D. Grosso, D. Deleruyelle, M. Putero, *Nanotechnology* **2018**, *30*, 025202.
[101] S. Eslava, M. R. Baklanov, C. E. A. Kirschhock, F. Iacopi, S. Aldea, K. Maex, J. A. Martens, *Langmuir* **2007**, *23*, 12811.
[102] C. Boissiere, D. Grosso, S. Lepoutre, L. Nicole, A. B. Bruneau, C. Sanchez, *Langmuir* **2005**, *21*, 12362.
[103] C. Millán, C. Santonja, M. Domingo, R. Luna, M. á. Satorre, *Astron. Astrophys.* **2019**, *628*, A63.
[104] J. A. Woollam, https://www.jawoollam.com/download/pdfs/rc2-brochure.pdf (accessed: August 2020).
[105] J. D. Bass, D. Grosso, C. Boissiere, C. Sanchez, *J. Am. Chem. Soc.* **2008**, *130*, 7882.

[106] M. C. Fuertes, S. Colodrero, G. Lozano, A. R. González-Elipe, D. Grosso, C. Boissière, C. Sánchez, G. J. de A. A. Soler-Illia, H. Míguez, *J. Phys. Chem. C* **2008**, *112*, 3157.
[107] F. N. Dultsev, *Electrochem. Solid-State Lett.* **1999**, *2*, 192.
[108] K. S. W. Sing, R. T. Williams, *Microporous Mesoporous Mater.* **2012**, *154*, 16.
[109] K. P. Mogilnikov, M. R. Baklanov, *Electrochem. Solid-State Lett.* **2002**, *5*, F29.
[110] J. Loizillon, B. Baumgartner, C. Sinturel, M. Abbarchi, B. Lendl, D. Grosso, *J. Phys. Chem. C* **2019**, *123*, 23464.
[111] A. Demessence, C. Boissière, D. Grosso, P. Horcajada, C. Serre, G. Férey, G. J. A. A. Soler-Illia, C. Sanchez, *J. Mater. Chem.* **2010**, *20*, 7676.
[112] M. Krishtab, I. Stassen, T. Stassin, A. J. Cruz, O. O. Okudur, S. Armini, C. Wilson, S. D. Gendt, R. Ameloot, *Nat. Commun.* **2019**, *10*, 3729.
[113] L. D. Salmi, M. J. Heikkilä, E. Puukilainen, T. Sajavaara, D. Grosso, M. Ritala, *Microporous Mesoporous Mater.* **2013**, *182*, 147.
[114] S. Eslava, L. Zhang, S. Esconjauregui, J. Yang, K. Vanstreels, M. R. Baklanov, E. Saiz, *Chem. Mater.* **2013**, *25*, 27.
[115] A. J. Cruz, I. Stassen, M. Krishtab, K. Marcoen, T. Stassin, S. Rodríguez-Hermida, J. Teyssandier, S. Pletincx, R. Verbeke, V. Rubio-Giménez, S. Tatay, C. Marti-Gastaldo, J. Meersschaut, P. M. Vereecken, S. De Feyter, T. Hauffman, R. Ameloot, *Chem. Mater.* **2019**, *31*, 9462.
[116] J. Silvestre-Albero, A. Silvestre-Albero, F. Rodríguez-Reinoso, M. Thommes, *Carbon* **2012**, *50*, 3128.
[117] D. Lässig, J. Lincke, J. Moellmer, C. Reichenbach, A. Moeller, R. Gläser, G. Kalies, K. A. Cychosz, M. Thommes, R. Staudt, H. Krautscheid, *Angew. Chem.* **2011**, *123*, 10528.
[118] T. Pauporté, J. Rathouský, *J. Phys. Chem. C* **2007**, *111*, 7639.
[119] M. Thommes, N. Nishiyama, S. Tanaka, in *Studies in Surface Science and Catalysis* (Eds: D. Zhao, S. Qiu, Y. Tang, C. Yu), Elsevier, New York **2007**, pp. 551–554.
[120] K. M. Krause, M. T. Taschuk, K. D. Harris, D. A. Rider, N. G. Wakefield, J. C. Sit, J. M. Buriak, M. Thommes, M. J. Brett, *Langmuir* **2010**, *26*, 4368.
[121] S. J. F. Herregods, K. Wyns, M. Mertens, R. Kemps, A. Buekenhoudt, V. Meynen, *Thin Solid Films* **2015**, *593*, 17.
[122] I. Stassen, M. Styles, G. Grenci, H. V. Gorp, W. Vanderlinden, S. D. Feyter, P. Falcaro, D. D. Vos, P. Vereecken, R. Ameloot, *Nat. Mater.* **2016**, *15*, 304.
[123] K. Zhang, L. Zhang, J. Jiang, *J. Phys. Chem. C* **2013**, *117*, 25628.

Timothée Stassin obtained his Ph.D. in 2019 at KU Leuven (Belgium) and was a doctoral fellow of the Research Foundation Flanders (FWO). At the KU Leuven Centre for Membrane Separations, Adsorption, Catalysis, and Spectroscopy (cMACS), he investigated the vapor-phase processing of metal–organic framework powders and thin films, with a particular focus on novel chemistries, deposition methods, and characterization techniques. His current interests as independent researcher include bridging the gap between high-tech academic research and low-tech field solutions, and the development of collaborative and multidisciplinary research platforms.

Rhea Verbeke obtained her Ph.D. in 2020 at KU Leuven (Belgium) and was a doctoral fellow of the Research Foundation Flanders (FWO). Her work at the KU Leuven Centre for Membrane Separations, Adsorption, Catalysis, and Spectroscopy (cMACS), targets the development of chemically robust water purification membranes for applications in harsh conditions. During her Ph.D., she conducted research at Yale University (US), the R&D department of DuPont Water Solutions in Tarragona (ES) and the Research Neutron Source of the Technical University of Munich (DE). She has pioneered the use of epoxide chemistry for membrane synthesis, and explored advanced physico-chemical characterization methods, including ERD and PALS.

Rob Ameloot obtained his Ph.D. in 2011 at KU Leuven (Belgium) and was a Fulbright postdoctoral fellow at UC Berkeley (US). He is currently a tenured professor at the KU Leuven Centre for Membrane Separations, Adsorption, Catalysis, and Spectroscopy (cMACS) and co-founder of the Leuven Institute for Micro- and Nanoscale Integration (LIMNI) launching in 2021. He was awarded ERC Starting and Proof-of-Concept grants to bring microporous materials from the chemistry lab into the microelectronics fab. In general, he is passionate about pushing the envelope in porous materials and process technology, with a healthy disregard for traditional subject boundaries.